PROTECTIVE EFFECTS OF *CARICA PAPAYA* LEAF EXTRACT ON THE GUT–LUNG AXIS IN ASBESTOS-EXPOSED RATS

U. Haider[*1], B. Aslam[*1], N. U. Khan[2], W. Nasir[3] and, [1]M. S. Tariq

[1]Institute of Physiology and Pharmacology, Faculty of Veterinary Science, University of Agriculture Faisalabad, Pakistan
[2]Department of Rehabilitation Sciences, Faculty of Medicine and Allied Health Sciences, The University of Faisalabad, Pakistan
[3]Department of Physiology, The University of Faisalabad
***Corresponding Authors' emails:** bilal.aslam@uaf.edu.pk ; 2020ag420@uaf.edu.pk

ABSTRACT

The gut-lung axis is a key regulator of host immunity illustrating the influence of gut microbiota on respiratory system through systemic and mucosal immune pathways. The purpose of this study was to evaluate the effect of asbestos-induced inflammation on the gut–lung axis by examining changes in gut microbiota composition, and to determine the impact of *C. papaya* extract in mitigating of induced inflammation and microbial dysbiosis. The study followed a completely randomized design-based experimental trial, employing a total of 32 male Albino Wistar rats weighing approximately 150-160g on average and aged 8 weeks. The experimental units were assorted randomly into four groups, namely Negative Control Group (receiving no induction or treatment), Positive Control Group (exposed to asbestos fibers through inhalation and oral ingestion), Standard treatment group (asbestos exposure + Naproxen 10 mg/kg b.wt orally) and Herbal Treatment Group (asbestos exposure + *C. papaya* extract 500 mg/kg body weight) orally daily. All experimental rats were maintained raised a period of two weeks (14 days). Fecal samples were collected to assess fecal consistency, gut microbiota composition by qRT-PCR, and short-chain fatty acid (SCFA) levels using FTIR. Bronchoalveolar lavage fluid (BALF) was obtained for cell count and mucus grading. Statistical assessment of numerical data employed repeated measure Analysis of Variance (ANOVA) followed by Tukey's Post hoc test with $p \leq 0.05$ considered a significant difference among all experimental groups. The FTIR results demonstrated improved absorption bands of SCFAs in Herbal Treatment group compared to other groups, with enhance hydrocarbon stretch patterns. The BALF smear showed high lymphocytic infiltrate in Positive Control Group compared to treatment groups, indicative of acute asbestos toxicity, and a marked decrease $(p \leq 0.05)$ in lymphocyte infiltrate in Herbal Treatment group, showing the effectiveness of *C. papaya* in immunomodulation. The qPCR results for microbial analyses showed a significant increase $(p \leq 0.05)$ in pathogenic bacterial strains and a subsequent decrease $(p \leq 0.05)$ in commensal microbiota in the Positive Control group compared to treatment groups, and this dysbiotic profile was restored to high commensal: low-to-pathogenic ratio in Herbal treatment group. The qRT-PCR results for genetic studies showed a significant upregulatory pattern $(p \leq 0.05)$ in Herbal treatment group after asbestos exposure, compared to a significant down-regulation $(p \leq 0.05)$ in Positive Control group, which was concomitant to the Histopathological observation where distorted mucosal layers in Positive Control group were parallelly were restored in Herbal treatment group with significant improvement in mucosal inflammatory changes and overall histoarchitecture. The obtained results suggest the therapeutic role of *C. papaya* extract in mitigating inflammation and partial restoration of dysbiosis associated with asbestos exposure.

Keywords: Microbiome, Oxidative Stress, Environmental Toxins, Dysbiosis, BALF

https://doi.org/10.36899/JAPS.2026.6.0138 Published first online August 19, 2026

INTRODUCTION

The gut–lung axis refers to the bi-directional relationship between the gut microbiota and the lungs (Yu, 2008). It is mediated through the immune system, microbial metabolites, and systemic circulation (Merchak and Gaultier, 2020). Gut microbes produce metabolites such as (Short Chain Fatty Acids) SCFAs that enter the bloodstream and reach the lungs. These metabolites regulate pulmonary immune responses and inflammatory processes, thereby influencing respiratory health and disease conditions. Beneficial gut bacteria (like *Lactobacillus* and *Bifidobacteria*) produce butyrate, propionate, and acetate (Portincasa *et al.*, 2022). Exogenous or endogenous metabolites which behave as toxins in the cell can induce inflammatory responses as self-defense mechanisms (Chen *et al.*, 2022; Su *et al.*, 2023). This inflammation can

also disturb gut microbiota composition by altering immune signaling, immune cell migration, and physiological stress responses (Hou *et al.,* 2024; Li *et al.*, 2024a). Immune cells activated within the gut can migrate systemically and mediate immune communication between the gut and lungs. The linkage between organ systems in disease conditions is established through this systemic circulatory migration of immune cells, which influences the microbial signaling and exacerbates pathogenic severity (Tulic *et al.*, 2016; Ding *et al.,* 2026).

Asbestos, known as the "Hidden Killer", poses a major threat due to its microscopic fibers and lack of warning signs. It causes thoracic, ovarian, laryngeal, and gastrointestinal tract cancer extending the spectrum of its detrimental health impacts (Smith and Wright, 1996). In the context of lung cancer, it is commonly believed that the inflammatory responses triggered by inhaling asbestos primarily affect the respiratory epithelium and lung parenchyma (Klebe e*t al.*, 2020). The lung parenchyma houses large cytosolic multi-protein complexes of innate immune system called inflammasomes, which act as sensors for the presence of pathogens and cellular damage (Vemula *et al.,* 2024). These inflammasomes establish the homeostatic boundary between lungs and gut, identifying pathogens and danger-related molecules (Zmora *et al.,* 2017; Wang et al., 2024b). They modulate the interleukins and antimicrobial peptides that are linked to gut microbial composition (Angosto-Bazarra *et al.*, 2022). Down-regulation of the Inflammasomes pathway leads to dysbiosis and stimulate goblet cells, which provide intestinal barrier in the form of mucus secretion (Shang *et al.,* 2024; Neurath *et al.,* 2025). Nod-like receptors containing pyrin and leucine-rich proteins also govern the secretion of mucus from goblet cells (Fusco et al., 2020; Wang *et al.,* 2025). Asbestos can disrupt the balance of gut bacteria, leading to dysbiosis characterized by an imbalance between beneficial and harmful microorganisms (Zandwijk *et al.,* 2024). This imbalance may result in increased intestinal permeability, inflammation, and a heightened risk of gastrointestinal diseases (Utembe and Kamng'ona, 2024, Li *et al.,* 2026).

Biomedical research is now focused on isolating and utilizing the bioactive compounds found in traditional herbal medicine (Khan *et al*., 2026). Among these, *C. papaya* is a notable choice for its alkaloid (carpaine), flavonoid (quercetin, kaempferol), phenolic acid, carotenoids and proteolytic enzyme (papain, chymopapain) constituents. These constituents exhibit strong antioxidant, anti-inflammatory, antimicrobial, anticancer, hepatoprotective, anti-diabetic, cardio-protective, wound-healing, and immunomodulatory effects through mechanisms such as free radical scavenging, enzyme inhibition, apoptosis induction, and immune regulation (Xu *et al*., 2025). Despite increasing evidence regarding asbestos-induced pulmonary inflammation and the importance of the gut-lung axis in respiratory diseases, limited studies have investigated the role of gut microbial dysbiosis in modulation of gut-lung axis signaling and disease pathogenesis. Previous research has mainly focused on the carcinogenic and fibrotic effects of asbestos on lung tissues, while the role of gut microbiota, inflammasome-mediated inflammation, and intestinal barrier dysfunction in asbestos toxicity remains poorly understood. The objective of the study was to investigate asbestos-induced gut microbial dysbiosis and inflammatory alterations in the gut-lung axis, and to evaluate the protective role of *C. papaya* extract in restoring microbial balance and reducing inflammation.

MATERIALS AND METHODS

Experimental Design: The study was conducted in January 2025 in Molecular and Cell Biology Post-Graduate Physiology Lab at the Institute of Physiology and Pharmacology, University of Agriculture Faisalabad. The study was conducted as a randomized controlled trial following CRD, where a total of 32 male Albino Wistar rats having an average weight of about 150-160 grams and aged 8 weeks of age, were reared in the Animal House facility at the institute according to guidelines given by the Animal Ethics Committee (UAF - DC. No. 1547/ORIC). The experimental units were divided into 4 groups, each group containing 8 rats (total N = 32, n = 8) including (i) Negative Control receiving normal diet and water, (ii) Positive Control, animals were exposed to asbestos fibers through inhalation and oral ingestion in specialized glass chamber for 2 hours daily over a period of 2 consecutive weeks. Inhalation exposure was maintained within OSHA limits (0.1 fibers/cm^3 as an 8-hour TWA; maximum 1.0 fibers/cm^3 for 30 minutes), verified by air sampling (Haider *et al.,* 2025). Oral ingestion doses were calculated according to body weight (mg/kg), (iii) Standard Treatment where asbestos-exposed received Naproxen 10 mg/kg was administered orally, and (iv) Herbal Treatment where asbestos exposure + ethanolic extract of *C. papaya* dose rate of 500 mg/kg body weight daily.

Acute Toxicity Assay: For acute toxicity assay, ethanolic extract of *C. papaya* was administered at the dose fractions of 100, 200, 300, 400, 500, 600, 700, and 800 mg. At the 500 mg dose, no significant alterations in behavioral patterns, including convulsions, paralysis, diarrhea, respiratory distress, weight loss, or lethargy, were observed (Haider *et al.,* 2026). (However, at higher doses, mild diarrhea, allergic reactions, and behavioral changes were reported. The acute toxicity assay indicated that 500 mg dose was safe and devoid of significant side effects, consistent with previously reported literature (Haider *et al.,* 2025).

C. papaya leaves extraction protocol: Leaves of *C. papaya* were collected from the botanical garden of University of Agriculture Faisalabad and subjected to shade drying. The dried leaves were then crushed and ground into a fine powder.

The powdered material was weighed and extraction was carried out by soaking one part powder in three parts of 70% ethanol for 48-72 hours. Following extraction, the mixture was filtered, and the filtrate was concentrated using a rotary evaporator. The resulting paste material was placed in an incubator at 60℃ for drying. The final dried extract was then stored in airtight centrifuge tubes for further analysis (Ali, 2024).

Body Weight and Fecal Consistency: Body weight was recorded on day 1, day 7, and day 14 of the experimental trial using an electronic digital weighing scale (SF-400) with a measurement range of 0.1 g to 10 kg. Stool consistency and frequency were monitored as indicators of gut motility function. Physical examination of fecal matter was performed daily in all experimental groups.

Fourier Transform Infrared Radiation (FTIR): FTIR spectroscopic analysis was performed using a PerkinElmer® FTIR spectrometer for the detection of SCFAs in fecal samples. Briefly, 100 mg of fecal sample was mixed with 100 µL phosphate-buffered saline and 100 µL of 1% HCl. The mixture was thoroughly homogenized, followed by addition of 100 µL chilled chloroform. The homogenate was allowed to stand for 1 hour, after which the upper layer was collected and stored for analysis (Liaqat *et al.,* 2024). Analyses of the samples were done at wide spectral range and at the resolution of $4cm^{-1}$ (Chakraborty *et al.,* 2024). The FTIR analysis were focused on identification of the different functional groups (C=O stretch, C–O stretch, C–H bond, and N–H linkage which will indicate the SCFAs) and their stretching in different groups of the experiment (Rumiyati *et al.,* 2024).

Broncho-alveolar Lavage Fluid analysis (BALF): Xylazine with dose rate of 0.01 mL and ketamine with dose of 0.05 mL were administered (intraperitoneally) under keen observation and care to all experimental groups rats. A small incision was given on the dorsal part of the trachea and 19-gauge sterilized needle filled with chilled saline was plunged into all segments of lungs. This fluid was retrieved gently about 5 times to collect the BALF, after repeated retrieved BALF was centrifuged at at 3×g at 4℃, and supernatants was taken into falcon tubes then stored at particular temperature (Bazzano *et al.,* 2020).

Differential Staining of BALF smear: The collected sample of BALF was centrifuged, and that resulted in pellet drop formation in the suspension which was then placed on the glass slide. After that with the help of another glass thin smear was produced and fixed with methanol for 1-2 minutes. A 100× oil-immersion lens was used for detailed examination, and a minimum of 30 cells were counted for differential cell analysis (Li *et al.,* 2024).

Gut microbial analysis by qRT-PCR: Fecal content was collected from ileo-cecal junction and immediately stored at -80℃ (Gazet, 1968). Genomic DNA was extracted using the FAVORGEN Stool DNA Isolation Mini Kit (Nadi *et al.,* 2015). The isolated DNA was subsequently stored at -20℃ and its quality and quantity were assessed using a Thermo Fisher Scientific NanoDrop™ spectrophotometer (Cat. No. N12391) by measuring the absorbance ratio at 260/280 nm (Salonen *et al.,* 2010). Intestinal tissues were preserved in TRIzol Reagent, followed by extraction of total mRNA. The isolated mRNA was subsequently reverse transcribed into cDNA using the RevertAid First Strand cDNA Synthesis Kit, and gene expression analysis was performed using quantitative real-time PCR. The following primers were used in the study (Table 1):

Table 1. Primer Sequences for qRT-PCR

Target Gene / Bacteria	Forward Primer (5' → 3')	Reverse Primer (5' → 3')
V2 Region (16S rRNA)	AGAGTTTGAGCCCGATCAG	TGCTGCCTCCCGTAGGAGT
Lactobacillus	AGCAGTAGGGAATCTTTCCA	CACCGCTACACATGGAG
Escherichia coli	GTTAATACCTTTGCTCATTGA	ACCAAGGGTATCTAATCCTGTT
Firmicutes	GGCAGCAGTAGGGAATCTTC	ACACTTAGAAACTCATCGTTT
Bifidobacteria	GTTAATACCTTTGCTCATTGA	CCACATCCAGCATACCAC
Gamma Proteobacteria	TGCCGCGTGTGTGAA	ACTCCCAGGCGGTCATTA
Enterococcus Faecalis	GCCATGCGCGGCATAACTG	CGCTTCTTTCCTCCGAGT
NOD2	GGAAACAACATTGGCAGCGT	TAACTGCCCAGCCGAAGAAG
Beta-actin	AAGAGAGGCATCCTGACCCT	ATGGCTACGTACATGGCTGG
CLDN2	TGGGGCTATTAGGCACATCG	AAGAGAGGCTTCAGGGCCTA
GPR41	AGCAGCGTCTTCTTCCTCAC	GGCTGCCAGGTTGACTATGT
TJP1	AAGGAGGTAGAGCGAGGCAT	GCTGACAGGTAGGACAGACG
OCLN	TTACGGCTACGGAGGGTACA	AGTCTCCCACCATCCTCTTGA
MUC2	CCTTCGACACCTAGCACC	TGGGGGAGTTGAGGGAGTAG

qRT-PCR was performed using Maxima SYBR Green/ROX qPCR Master Mix (2X) (Ref. K0221, Lot. 01134497) in 0.1 mL 8-strip PCR tubes (Cat. No. 403102). Gene expression analysis was carried out following the manufacturer's protocol. The thermal cycling conditions included an initial denaturation step at 95℃ for 1 minute, followed by 40 cycles consisting of denaturation at 95℃ for 30 seconds, annealing at 58.4℃ for 20 seconds, and extension at 72℃ for 60 seconds (Bansal *et al.,* 2023).

Histopathology: Large intestinal tissues were stained using Masson's trichrome staining (Clarke *et al.*, 2024) and lung tissues were stained with hematoxylin and eosin (Ankle and Joshi, 2011). Microscopic examination was performed using a light microscope (IRMECO GmbH & Co., Model IM-910, Germany), and images were captured using an attached TOUPCAM UCMOS14000KPA microscope camera with ToupView software v3.7. Photomicrographs were recorded for further evaluation.

Statistical Analysis: The study was conducted using CRD where data were analyzed using A repeated measure ANOVA followed by Tukey's post hoc test to determine statistical significance ($p \leq 0.05$) among all groups. Graphical representations were generated using GraphPad Prism software (v8.1).

RESULTS

Body Weight: The body weight was measured on day 1, day 7, and day 14 of the experimental trial. The obtained data were subjected to statistical analysis, which revealed a significant reduction *($p \leq 0.05$)* in body weight in the Positive Control group compared to Negative Control at days 7 and 14. In Contrast to a significant restorative increase *($p \leq 0.05$)* in body weight was observed in both the Standard and Herbal Treatment group compared to the Positive Control group (Table 2).

Table 2. Body Weight (g) changes in experimental groups over the study period

Group	Day 1 M±SE	Day 7 M±SE	Day 14 M±SE
Negative Control	155.0 ± 2.89^{a}	$176.0 \pm 3.46^{a,b}$	210.0 ± 2.89^{b}
Positive Control	149.3 ± 2.03^{a}	140.3 ± 0.88^{b}	$150.7 \pm 1.45^{a,c}$
Standard Treatment	155.0 ± 1.73^{a}	$160.7 \pm 1.45^{a,b}$	178.0 ± 2.08^{c}
Herbal Treatment	153.0 ± 1.73^{a}	$159.3 \pm 4.36^{a,b}$	172.0 ± 4.36^{c}

Values are presented as mean ± SEM. Different superscript letters within a row indicate significant differences among time points ($p \leq 0.05$)

Fecal Consistency: In the Negative Control group, normal fecal pellets were observed with no detectable asbestos fibers. In contrast, the positive control group exhibited frequently loose stools with a high presence of asbestos fibers. However, the Standard Treatment and Herbal Treatment groups showed soft fecal consistency with only a few detectable asbestos fibers.

Short-Chain Fatty Acids (Functional Metabolites) assessed by FTIR: FTIR analysis was used to identify functional groups associated with SCFAs. Characteristic absorption bands included C=O stretching (1700-1725 cm^{-1}) indicating acetic acid, O–H stretching (2500-3300 cm^{-1}) representing fatty acids in general, C–H stretching (2850-2960 cm^{-1}) associated with butyric acid, and C–O stretching (1150-1250 cm^{-1}) corresponding to SCFA functional groups. All the observations and findings are in Figure 1 and Table 3.

a) Spectral profile of SCFAs in Negative Control group of showed strong stretching O–H having wavelength number 3317 cm^{-1}, stretching of C–H with wavelength number of 2978 cm^{-1}, peak intensive stretching of C=O with wavelength number 1638 cm^{-1}, and there was a distinct stretch in bond of C–O with wavelength number 1046 cm^{-1}.

b) The Spectral profile of SCFAs in Positive Control group showed that there was weak bond in stretching of O–H with wavelength number of 3278 cm^{-1}, and reduced bond stretching in C=O while mild bond stretching in C–H with wavelength number 2978 cm^{-1}, and a moderate stretch C–O signal with wavelength number of 1045 cm^{-1}, indicating decreased SCFA content.

c) Spectral profile of SCFAs in Standard Treatment group showed stronger bond stretching of O–H with wavelength number of 3330 cm^{-1}, clear bond stretching in between the C–H with wavelength number of 2976 cm^{-1}, similarly a prominent peak bond stretching occurred in between the C=O having wavelength of 638 cm^{-1}, and well-defined stretching in between the C–O having wavelength number 1306–1045 cm^{-1} that reflects the SCFA restoration.

d) The Spectral profile of SCFAs in Herbal Treatment group showed moderately strong stretching O–H having the wavelength number of 3317 cm^{-1}, while the bond stretching in C–H with wavelength of 2978 cm^{-1} as compared to Herbal Treatment group the Standard Treatment group the stretching intensity of C=O, and well-defined multiple C–O peaks (1306-1045 cm^{-1}).

Table 3. Overlay of FTIR Spectra for SCFAs

Observed Wavenumber (cm^{-1})	Functional Group / Bond Type	Assignment / Relevance to SCFAs	Negative Control	Positive Control	Standard Treatment	Herbal Treatment
3317–3330	O–H stretch (H-bonded)	Broad band; hydroxyl group of carboxylic acids; present in all fatty acids	3317 (strong)	3278 (weak)	3330 (strong)	3317 (moderate)
1700–1725	C=O stretch (carboxylic acid)	Strong, sharp; indicates acetic acid and other SCFAs	1638 (intense)	1638 (weak)	1638 (strong)	1638 (strong)
2 850–2960	C–H stretch (alkyl groups)	Aliphatic chains; linked to butyric acid	2978 (clear)	2978 (mild)	2976 (clear)	2978 (moderate)
1150–1250 / 1306–1045	C–O stretch (carboxyl group)	Present in all SCFAs; multiple peaks from C–O bonds	1046 (distinct)	1045 (moderate)	1306–1045 (sharp)	1306–1045 (multiple, well-defined)
~1638	C=O stretching / COO^- asymmetric stretch	Shifted due to conjugation/H-bonding in SCFAs	1638 (intense)	1638 (non-intensive)	1638 (strong)	1638 (strong)

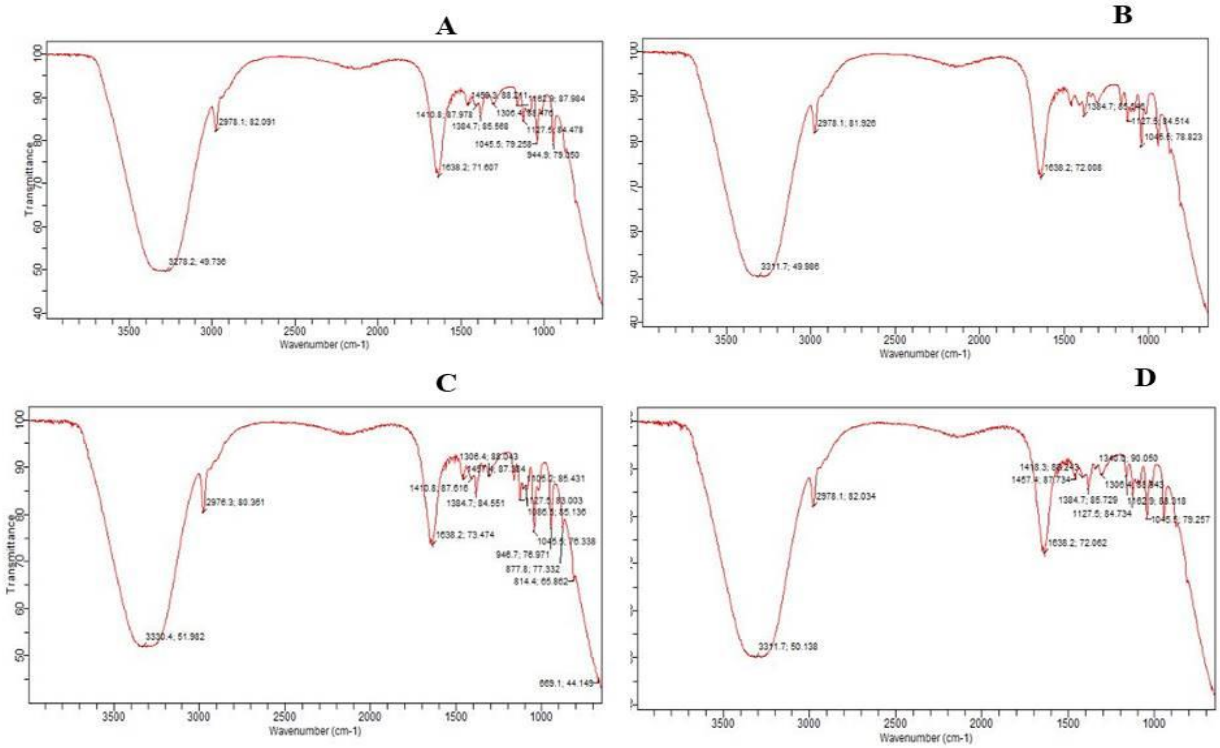

Figure 1. The FTIR representative spectrum that display the peaks of specific functional groups, their bond linkage, stretching lengths that are associated with the SCFAs. Bands with specific wavelengths showed different stretching like C=O bond stretching indicative for carboxylic acids, 0-H stretching bands, and stretching patterns of the C-H. A) showed the FTIR Spectrum with wavelengths of the Control Negative Group, B) showed the FTIR Spectrum with wavelengths of the Control Positive Group, C) showed the FTIR Spectrum with wavelengths of the Standard Treatment Group, and D) showed the FTIR Spectrum with wavelengths of the Herbal Treatment Group. It depicts the differences in the peak intensity, shifts of wavelengths among the different groups in SCFAs.

Bronchoalveolar Lavage Fluid (BALF) Analysis: BALF analysis help in cell counting (Differential) to identify the inflammatory condition, any infectious agent, allergens, and pulmonary neoplastic. For this purpose almost 250-300 cells randomly counted in selected specific microscopic fields (by using oil immersion lens)it was observed that different cell count was noted among all groups. Variations in the percentage of different cell populations were observed among all experimental groups, indicating inflammatory changes associated with asbestos inhalation. Table 4 presents the types of cells identified their percentages, and their morphological characteristics in normal and asbestos-exposed groups. Table 5 summarizes the grading, color, and volume of mucus obtained from the BALF of the Negative Control, Positive Control, Standard Treatment, and Herbal Treatment groups (Holcombe *et al.,* 2006).

Table 4. Effect of Asbestos Exposure on Different blood cell types in BALF

Groups	Macrophages	Neutrophils	Lymphocytes	Eosinophils'	RBC
Control Negative	65-70	2	3	1	Absent
Control Positive	80-85	12-15	8-10	3	Occasionally present
Standard Treatment	70-75	8-10	4-5	1	Absent
Herbal Treatment	72-80	3	6-7	2	Absent
	Large-sized cells, round nucleus, Pale blue cytoplasm	Medium sized cells, Multi-lobed nucleus, Pinkish cytoplasm	Small-sized cell, blue cytoplasm, round nucleus major portion	Large-sized cells, bi-lobed nucleus	Biconcave shape, no nucleus

Table 5. Grading of mucus collected from BALF

Groups	Mucus grade (0-3)	Color	Volume
Negative Control	0	Clear fluid presence	13 µL
Positive Control	3 (High)	Gelatinous	110 µL
Standard Treatment	2 (Moderate)	Slightly Cloudy	44 µL
Herbal Treatment	2 (Moderate)	Viscous	57 µL

Gut Microbiota analysis by qRT-PCR: A significant *($p \leq 0.05$)* two-fold increase in the abundance of pathogenic bacterial taxa, including *Escherichia coli (E. coli)*, *Campylobacter*, *Proteobacteria*, *Enterococcus faecalis*, and *Firmicutes* was observed in the Positive Control group compared to the Negative Control. Contrastingly, both Treatment groups demonstrated marked improvement *($p \leq 0.05$)* in gut microbial composition, characterized by a relative reduction and fold-change expression of these pathogenic bacteria (Figure 2). On the other hand, the commensal bacterial populations including *Lactobacillus* and *Bifidobacterium* were significantly reduced *($p \leq 0.05$)* in the Positive Control group. The administration of treatment resulted in significant upregulation *($p \leq 0.05$)* and restoration of these commensals in Herbal Treatment group compared to Positive Control (Figure 3). The relative abundance of *Enterococcus faecalis* (38%), *Campylobacter* (29%), *E. coli* (33%), and *Proteobacteria* (34%) was markedly elevated in the Positive Control compared to all other experimental groups. Contrastingly, in Positive Control group the beneficial bacterial were reduced having 18 % of *Bifidobacterium*, 17% of *Lactobacillus* (17%), and 18 % of *Firmicutes* (18%). Conclusively it was suggested that *C. papaya* has capacity to restore homeostasis of gut micro biome and microenvironment of intestine.

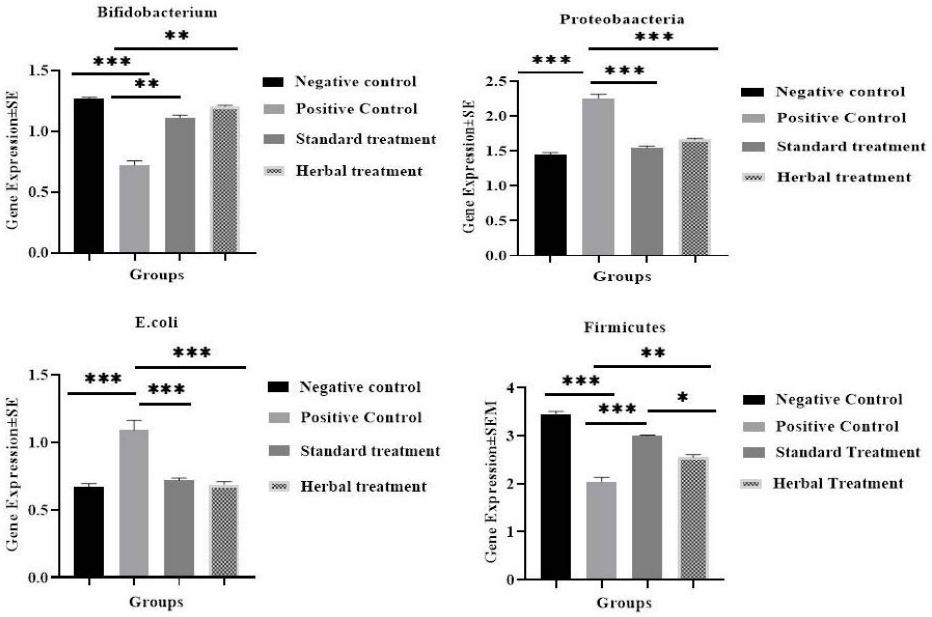

Figure 2. Fecal DNA was analyzed by qRT-PCR to quantify the abundance of Bifidobacteria, Proteobacteria, Escherichia coli, Firmicutes in Negative Control, Positive Control, Standard Treatment, and Herbal Treatment groups. Data are presented as fold-change relative to Negative Control group, calculated using the 2^–ΔΔCt method. The results reveal highly significant differences (p≤0.05) in microbial abundance patterns, indicating marked dysbiosis in Positive Control group and partial or complete restoration of microbial balance following treatment interventions.

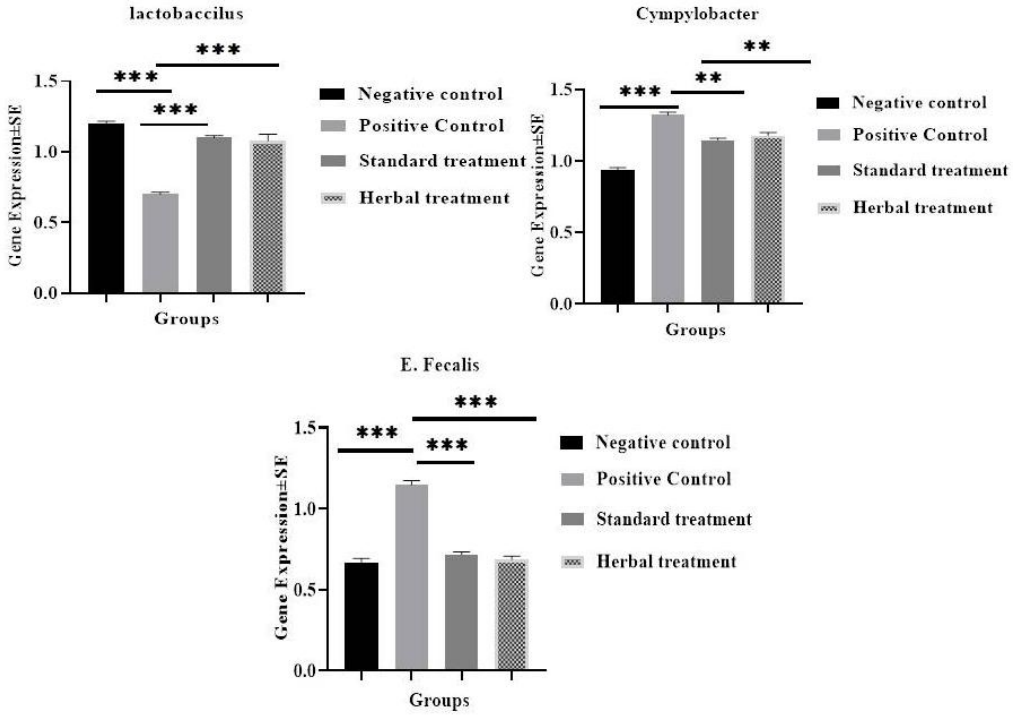

Figure 3. Fecal DNA was analyzed by qRT-PCR to quantify the abundance of Lactobacillus, Campylobacter, and Enterococcus faecalis in the Negative Control, Positive Control, Standard Treatment, and Herbal Treatment groups. Data are presented as fold-change relative to Negative Control group, calculated using the 2^–ΔΔCt method. The results revealed highly significant differences (p≤0.05) in microbial abundance patterns, indicating marked dysbiosis in the Positive Control group and partial or complete restoration of microbial balance following treatment interventions.

Gene Expression analysis of Gut Barrier and Immune Regulatory Genes:

NOD2: qRT-PCR analysis revealed significant downregulation *($p \leq 0.05$)* of NOD2 expression in the Positive Control group compared to Negative Control group. However, in Standard Treatment group and Herbal Treatment group the expression of NOD2 was elevated significantly *($p \leq 0.05$)* as shown in Figure 4.

***TJP1*:** Similarly the significant *($p \leq 0.05$)* downregulation of TJP1 *in Positive Control group*. However, the Herbal Treatment group significant *($p \leq 0.05$)* increase (2-fold upregulation) in TJP1 expression as shown in Figure 4.

MUC2: Similarly the MUC2 expression was significantly *($p \leq 0.05$)* reduced in Positive Control group as compared to the other experimental groups. While in Standard Treatment group and Herbal Treatment group the expression level of MUC2 was upregulated significantly *($p \leq 0.05$)* which is the indicative that the functioning of the mucosal barrier improved as in Figure 4.

OCLN: The expression level of OCLN was significantly downregulated *($p \leq 0.05$)* in Positive Control group compared to Negative Control group. Administration of *C. papaya* significantly increased *($p \leq 0.05$)* OCLN expression, indicating restored tight junction integrity..

GPR41: The expression of GPR41 was significantly reduced *($p \leq 0.05$)* in Positive Control group, exhibiting approx. 2-fold downregulation. In contrast, both treatment groups demonstrated significant upregulation of GPR41 expression compared to Positive Control group.

CLDNs: Expression of CLDNs was significantly reduced *($p \leq 0.05$)* in Positive Control group. However, both Standard and Herbal Treatment groups exhibited elevated expression levels of CLDNs *($p \leq 0.05$)* indicating improved intestinal barrier integrity (Figure 4).

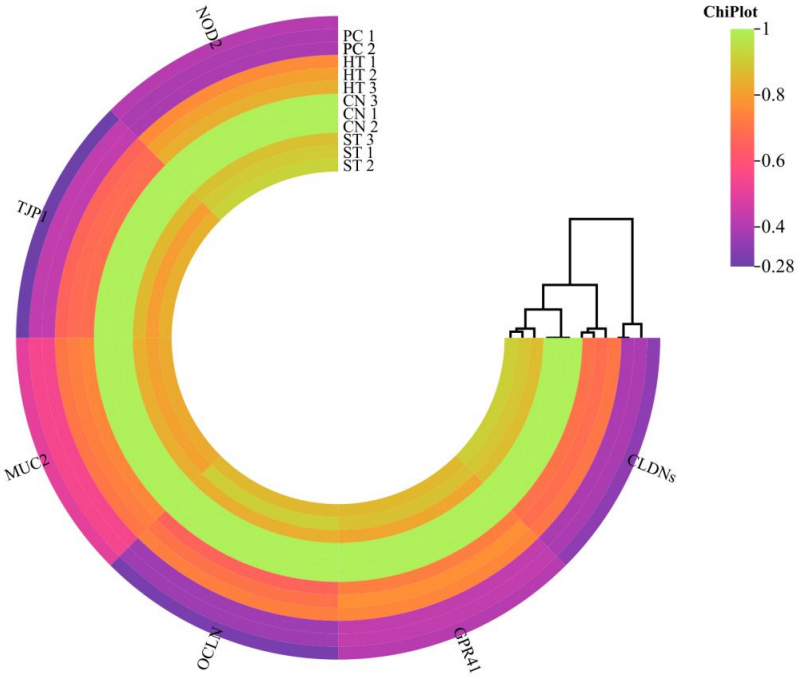

Figure 4. Heat map showing the gene expression levels in Negative Control, Positive Control, Standard Treatment, and Herbal Treatment groups. A significant downregulation ($p \leq 0.05$) of NOD2, TJP1, MUC2, OCLN, GPR41, and CLDNs was observed in Positive Control group, and subsequent upregulation in the Treatment Groups was seen after treatment administration.

Histology of Large Intestinal tissue: In the Negative Control group, the large intestine tissue exhibited an intact mucosal lining with well-organized crypt architecture, normal submucosal, and muscularis layers (15.16 ± 5.83 µm), and an even distribution of goblet cells with no evidence of goblet cell depletion or inflammation (inflammation score: 0), as shown in

Figure 6. Contrastingly, the Positive Control group demonstrated marked histopathological alterations, including crypt distortion, goblet cell depletion, mucosal hyperplasia in response to acute celluar degeneration and epithelial sloughing, and increased thickness of submucosa (28.92 ± 7.93 µm), accompanied by severe inflammation (inflammation score: 3).

There were considerable improvement were noticed in Standard Treatment group organization of the crypts improved, integrity of the epithelium was maintained, and number of goblet cells increased, the thickness of sub mucosal portion (18.44 ± 2.55 µm) was reduced and inflammatory changes were mild with inflammation score: 1 in comparison to Positive Control group. However, in the Herbal Treatment group number of the goblet cells were restored, thickness of the sub mucosa was decreased (21.44 ± 0.45 µm), epithelium gaining its intactness, but mild sloughing and inflammation was moderately observed with inflammation score: 2 and mild epithelial sloughing were still evident, as shown in Figure 5.

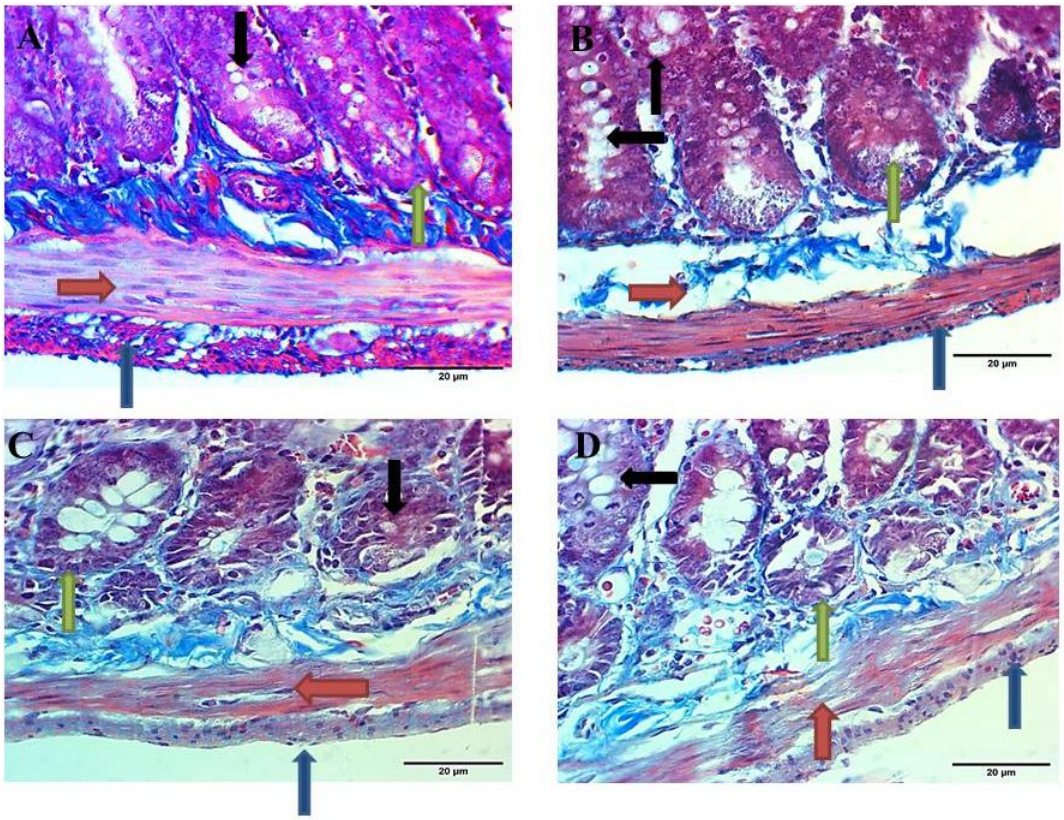

Figure 5. Photomicrograph captured at 40X (microscopic view) of the colon tissue of large intestine that was stained with Masson Trichrome and by using ImageJ (software) the thickness and mucosal length was measured In Figure A) represents the Masson Trichrome staining of Negative Control group while the Positive Control group Masson Trichrome staining was represented with B), the Masson Trichrome staining of Standard Treatment group was represented with C) and D) showed the Masson Trichrome staining of Herbal Treatment group. In the labeled figure Black arrows represents the show goblet cells, mus-cularis represented by red arrows, mucosal glands, are represented in green arrows and blue arrows mark the epithelium.

Histology of Lung tissue: *Negtive Control group showed the normal* architecture of pulmonary tissue exhibited that the alveolar walls were intact with normal septum. However, marked Histopathological changes were being in Positive Control group including the alveolar wall destruction, interalveolar septum become thickened which was the indicative of pulmonary injury. While there was moderate restoration, noticeable reduction in the thickness of septum of alveoli and restoration of the integrity of alveoli in Standard Treatment group and Herbal Treatment group which suggested that the partial recovery in the architecture of lung tissue. as in Figure 6.

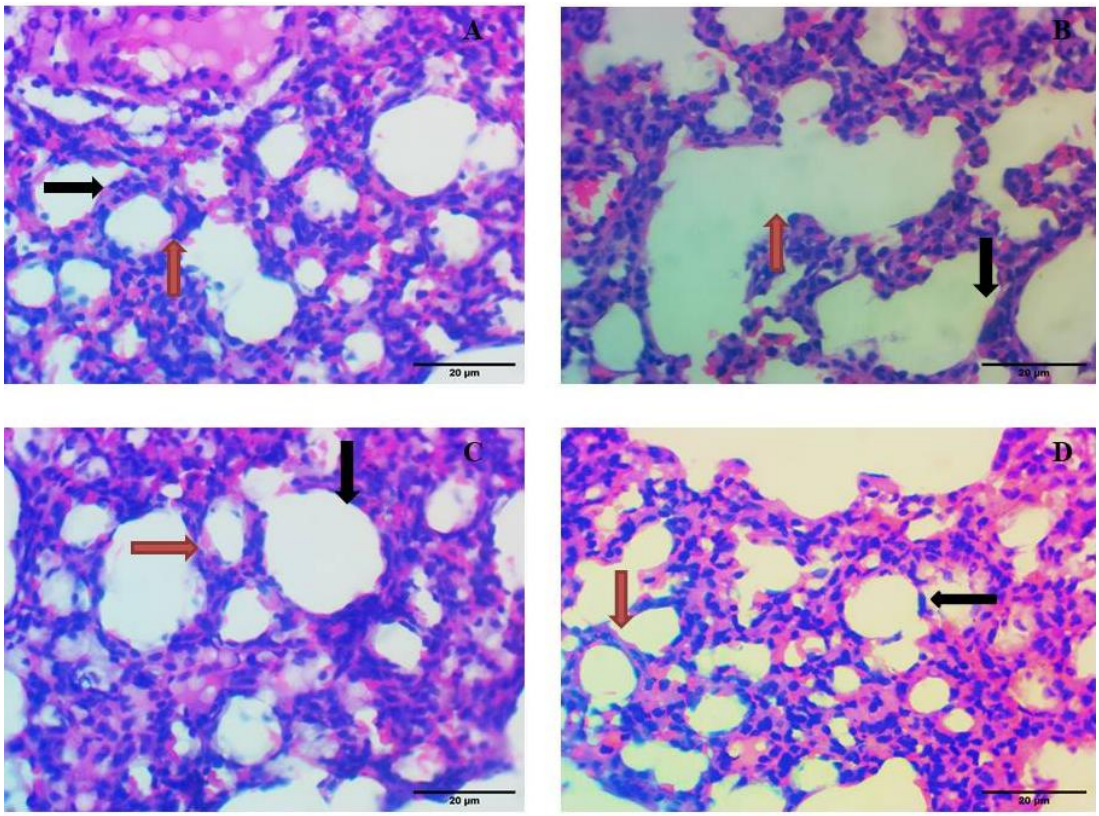

Figure 6. Photomicrograph captured at 40X (microscopic snap) H&E staining of the lung tissue. The histological structure of Negative Control group shown in A) while the histological deviation in the structure of lung tissue of Positive Control group presented in B) histological presentation of the Standard Treatment group presented in C) and the H&E staining of the lung tissue of Herbal Treatment group presented in D). Alveolar septum marked by Black arrow, s show the, and show the alveolar wall marked with red arrows.

DISCUSSION

The present study shows that asbestos exposure has a number of different effects on both lung and gut systems, including the induction of lung inflammation, gut microbial dysbiosis and Histopathological alterations. The BALF analysis showed significant changes in the cell composition and alveolar microenvironment. BALF analysis revealed an increased in the mucus volume, change in color and increased cells in Positive Control group compared to other groups (Shukla *et al.*, 2006). Excessive mucus was removed due to the presence of papain which is a major proteolytic enzyme of C. papaya in Herbal Treatment group. The results are similar to those from previous studies that found asbestos fibers play a role in triggering inflammation and oxidative stress in the lungs (Mossman *et al.*, 2011). Lung tissue also showed evidence of the asbestos causing disruption to its architecture, such as destruction of the alveolar walls and thickening of the interalveolar septa. Histopathological evidence indicated structural and functional recovery of lung tissue and these lesions were significantly reduced in both treatment groups. The bioactive compounds present in C. papaya showed a beneficial effect on the histological parameters by decreasing the oxidative stress and inflammation, thus preventing further damages of the tissues and promoting the repair process (Otarov *et al.*, 2025). The results show that asbestos exposure leads to both gut and lung inflammation and dysbiosis. These pathological changes are reversed by Standard and Herbal Treatments further indicating their importance in the pathogenesis caused by oxidative stress (Khan *et al.*, 2025). Importantly, the same Standard Treatment benefits were observed with the Herbal Treatment, supporting its use as a counter or alternative treatment (Wang *et al.*, 2024a).

Simultaneously, the gut microbiota analysis showed strong evidence of asbestos' systemic effects (Liu and Chen, 2017). Pathogenic and pro-inflammatory bacteria, such as E. coli, Campylobacter, Enterococcus faecalis, Proteobacteria and Firmicutes, had significantly increased ($p \leq 0.05$) populations in the Positive Control group. A significant decrease in beneficial commensals was seen such as Lactobacilli and Bifidobacteria in the presence of the asbestos fibers (Xu et al., 2025). This is a microbial imbalance that represents a disturbed environment in the intestines, probably due to systemic

inflammation and oxidative stress (Mostafavi Abdolmaleky and Zhou, 2024). C. papaya alkaloids have been shown to possess antimicrobial and immunomodulatory properties that could play a role in maintaining the microbial balance and minimizing tissue damage caused by toxins. In the treatment, the microbial balance was very well restored ($p \leq 0.05$) with a decrease in the pro-inflammatory taxa and an increase in beneficial bacteria in C. papaya. Interestingly, the Lactobacillus and Bifidobacteria populations were found to be significantly increased ($p \leq 0.05$) in the Herbal Treatment group, which indicates the potential effectiveness of C. papaya extract in restoring the microbial balance (Giambò *et al.,* 2022). These indicates that manipulation of the gut microbiota may be a therapeutic target for toxin-induced pathologies.

Additionally, changes in microbiota were confirmed by FTIR analysis of fecal samples, using biochemical signatures of SCFAs. The Positive Control group presented with its absorption bands being lower in intensity as seen in relation to the functional groups of the SCFAs (e.g., O-H, C=O, and C-O stretches), reflecting decreased production of SCFAs Chalova *et al.,* 2023). In contrast, the Standard and Herbal Treatment groups had greater and more widespread peaks, which correlated with greater synthesis of SCFAs. The beneficial gut microbes are supported by the high level of polyphenol, dietary fibers and flavonoids in C. papaya, leading to an increased production of SCFAs.

The results for gut microbial profiling revealed significant alterations in the microbial composition in all groups. The dysbiotic profile in Positive Control group suggests that asbestos exposure disrupts gut microbial homeostasis, favoring the proliferation of harmful bacteria. Decline in probiotic populations indicates a compromised gut environment, likely linked to inflammation and oxidative stress induced by asbestos. The study further evaluates the therapeutic efficacy of *C. papaya* in mitigating these effects (Mazumder and Hussain, 2024). These findings underscore the role of gut microbial metabolites in maintaining intestinal and systemic health (Yan et al., 2023). The current study hypothesized that exposure to asbestos particles markedly altered the expression of genes involved in stability of the intestinal histoarchitecture, mucosal immunity, and microbial signaling. The findings of gene expression analysis signify the protective role of the *C. papaya* extract in maintaining the gut homeostasis, and communication between the gut-lungs axis (Pang *et al.*, 2025). NOD2 gene modulates innate immune response and serves as a sensor of microbial peptidoglycans, responsible for triggering anti-microbial response upon peptidoglycan exposure (Strober and Watanabe, 2011). TJP1 acts as an intestinal tight-junction regulatory protein and is responsible for maintaining membrane permeability, disabling entrance of any pathogenic agents from mucosal membrane into circulation (Ulluwishewa *et al.*, 2011). MUC2 is a key mucin protein essential for mucus production and maintenance of the intestinal mucosal barrier. OCLN and CLDNs are critical structural components of tight junctions that regulate intestinal integrity and paracellular permeability (Moonwiriyakit *et al.,* 2023). The GPR41 gene is activated by the SCFAs and its downregulation suggests impaired microbial metabolite signaling (Zhan *et al.,* 2019). The findings indicate that asbestos exposure caused dysregulation of genes associated with intestinal barrier integrity, mucosal protection, and host-microbiota signaling pathways. The homeostasis of the gut barrier has been disrupted due the downregulation of the genes like GPR41, NOD2, OCLN1, MUC2, TJP1, and CLDNs. The current study showed that the herbal extract have protective effect in mitigating the inflammation, upregulation of the genes responsible for the maintenance of the gut integrity and intestinal barriers.

The current findings of SCFAs, biochemical analysis, molecular examination are further supported by the Histopathological and microscopic insights. Ingestion of the asbestos particles damages the mucosa of the large intestine, crypts becomes distorted, and depleted goblets cells, and sloughing of the epithelium. Due to potent therapeutic potential of *C. papaya* the partial restoration of the structural intestine and lung tissues had been reported (Erben *et al*., 2014).

Conclusion: It was concluded from the study that asbestos has severe effects on the production of SCFAs , gut microbiota dysbiosis, oxidative stress induced inflammation in the lung tissues, and marked Histopathological changes in both intestine and lungs tissue. It was noted that treatment with standard commercial drug and herbal extract have been effective in reducing the inflammation, maintaining the gut balance, and metabolites produced by SCFAs, and improving the integrity of the intestinal barrier. The microscopic examination of the lung and intestine tissues further support the protective effect of the *C. papaya* and making a promising strong natural therapeutic candidate for future translational medicine.

Limitations: There are certain limitations of this study due to budgetary constraints that include 16S rRNA sequencing, met genomics studies, dysbiosis indexing, NGS sequencing. Similarly, due limited cost the qRT-PCR and FTIR analyses were done as an alternative to the GC-MS and protein study. The phytochemicals of *C. papaya* were not employed, and animal allocation was conducted in a predetermined manner due to exposure chamber logistics.

Future Direction: Future studies should incorporate metagenomic and functional gene analyses related to SCFA biosynthesis, along with comprehensive microbial taxonomic profiling. Validation of SCFA quantification using GC-MS is also recommended for improved analytical accuracy.

Funding: None

Conflict of interest: None

Authors' contributions: All the authors contributed in conceptualization, drafting, proofreading, study design and writing.

Acknowledgment: We extend our sincere gratitude to Institute of Physiology and Pharmacology, Faculty of Veterinary Science and especially Dr. Muhammad Naeem Faisal for their invaluable support in providing all necessary equipment, chemicals, animal housing, and working facilities required for the successful completion of this research. Their generous contributions and resources played a crucial role in facilitating our work and ensuring its progress.

REFERENCES

Ali, L (2024). Unraveling the combinational approach for the antibacterial efficacy against infectious pathogens using the herbal extracts of the leaves of *Dodonaea viscosa* and fruits of *Rubus fruticosus*. Agrobiol Rec. 16: 57–66. https://doi.org/10.47278/journal.abr/2024.012

Angosto-Bazarra, D., C. Molina-López and P. Pelegrín (2022). Physiological and pathophysiological functions of NLRP6: pro- and anti-inflammatory roles. Commun Biol. 5: 1–8. https://doi.org/10.1038/s42003-022-03491-w

Ankle, M.R and P.S. Joshi (2011). A study to evaluate the efficacy of xylene-free hematoxylin and eosin staining procedure as compared to the conventional hematoxylin and eosin staining: An experimental study. J Oral Maxillofac Pathol. 15: 161–167. https://doi.org/10.4103/0973-029X.84482

Bansal, R., D.R. Haviland and W.B. Hunter (2023). Selection and validation of reference genes for quantifying gene expression in the Gill's mealybug. J. Econ. Entomol. 116: 2166–2172. https://doi.org/10.1093/jee/toad179

Bazzano, M., L. Laghi, C. Zhu, G.E. Magi, B. Tesei and F. Laus (2020). Respiratory metabolites in bronchoalveolar lavage fluid (BALF) and exhaled breath condensate (EBC) can differentiate horses affected by severe equine asthma from healthy horses. BMC Vet Res. 16:1–9. https://doi.org/10.1186/s12917-020-02446-9

Chakraborty, A., M. Kumar and S.A. Ali (2024). Identification and characterization of *Carica papaya* using FTIR and UV spectroscopy: A microemulsion analysis. Afr J Bio Sc. 6: 6981–7008. https://doi.org/10.48047/AFJBS.6.10.2024.6981-7008

Chalova, P., A. Tazky, L. Skultety, L. Minichova, M. Chovanec, S. Ciernikova, P. Mikus and J. Piestansky (2023). Determination of short-chain fatty acids as putative biomarkers of cancer diseases by modern analytical strategies and tools: A review. Front Oncol. 13: 1–23. https://doi.org/10.3389/fonc.2023.1110235

Chen, X., C. Chen and X. Fu (2022). Hypoglycemic effect of the polysaccharides from Astragalus membranaceus on type 2 diabetic mice based on the "gut microbiota-mucosal barrier". Food Funct. 13(19): 10121–10133. https://doi.org/10.1039/d2fo02300h

Clarke, E., A. Bajaka, A. Sm, K. Balawender, A. Wawrzyniak and A. Zytkowski (2024). Application of histochemical stains in anatomical research : A brief overview of the methods. Transl Res Anat. 35: 1-6. https://doi.org/10.1016/j.tria.2024.100294

Ding, N., H. Wu, Y. Hua, R. Hua, B. Li, Y. Xie, Y. Xiong, T. Bai, X. Shi, T. Shen, P. Liu, J. Liu, X. Yang, Y. Xu, Z. Meng, B. Lan, J. Zhou, B. Liu, J. Y. Shyy, Z. Yuan, Y. Wu and T. Li (2026). Gut microbiota-derived isovaleric acid alleviates atrial fibrillation by suppressing GSDME-dependent pyroptosis. Cell Metab. 38(2): 370–387. https://doi.org/10.1016/j.cmet.2025.12.017

Erben, U., K.D. Loddenkemper, S. Spieckermann, D. Haller, M.M. Heimesaat, M. Zeitz, B. Siegmund and A.A. Kühl (2014). A guide to histomorphological evaluation of intestinal inflammation in mouse models. Int J Clin Exp Pathol. 7:4557–4576. doi: PMC4152019/pdf/ijcep0007-4557

Fusco, R., R. Siracusa, T. Genovese, S. Cuzzocrea and R. Di Paola (2020). Focus on the role of NLRP3 inflammasome in diseases. Int J Mol Sci. 21:1–25. https://doi.org/10.3390/ijms21124223

Gazet, J.C (1968). The surgical significance of the ileo-caecal junction. Ann. R. Coll. Surg. Engl. 43:19–38. doi: PMC2312254/pdf/annrcse00254-0026

Giambò, F., C. Costa, M. Teodoro and C. Fenga (2022). Role-playing between environmental pollutants and human gut microbiota: A complex bidirectional interaction. Front Med. 9: 1–10. https://doi.org/10.3389/fmed.2022.810397

Haider, U., B. Aslam, S.U. Hassan and Z. ud D. Sindhu (2025). Immune modulatory potential of *Carica papaya* against asbestos-induced acute lung injury through down-regulation of NF-kB and MAPK pathways. Toxicol Res. 14(5):1-11. https://doi.org/10.1093/toxres/tfaf140

Haider, U., M. Ahmad, W. Nasir, N.U. Khan, M.S. Tariq, B. Aslam, S.U. Rehman and J. Sun. (2026). Therapeutic potential of *Carica papaya* (L.) extract on NRF2/KEAP1 and apoptotic pathways in asbestos-induced lung toxicity. Food Sci Nutr. 14: e71984. https://doi.org/10.1002/fsn3.71984

Holcombe, S.J., N.E. Robinson, F.J. Derksen, B. Bertold, R. Genovese, R. Miller, H.D.E.F. Rupp, E.A. Carr, S.W. Eberhart, D. Boruta and J.B. Kaneene (2006). Effect of tracheal mucus and tracheal cytology on racing performance in Thoroughbred racehorses. Equine Vet. J. 38: 300-304. https://doi.org/10.2746/042516406777749191

Hou, J., H. Gong, Z. Gong, X. Tan, X. Qin, J. Nie, H. Zhu and S. Zhong (2024). Structural characterization and anti-inflammatory activities of a purified polysaccharide from fruits remnants of Alpinia zerumbet (Pers.) Burtt. et Smith. Int J Biol Macromol. 267(2):131534. https://doi.org/10.1016/j.ijbiomac.2024.131534

Klebe, S., J. Leigh, D.W. Henderson and M. Nurminen (2020). Asbestos, smoking and lung cancer: An update. Int. J. Environ. Res. Public Health 17(1):1-23. https://doi.org/10.3390/ijerph17010258

Khan N.U., S.U. Hassan, B. Aslam and S. Umer (2025). *Ficus carica* leaf extract ameliorates cardiac injury through Nrf2/Keap1 pathway activation and dual oxidase inhibition. Iran J Basic Med Sci. 28(12): 1679-1690. https://dx.doi.org/10.22038/ijbms.2025.88664.19148

Khan N.U., S.U. Hassan, B. Aslam and S. Umer (2026). Investigating the therapeutic potential of *Ficus carica* leaves extract in a rat model of induced myocardial infarction. J Anim Plant Sci. 36(3): 861-871. https://doi.org/10.36899/JAPS.2026.3.0070

Li, G., Y. Qiao, Q. Wang, X. Zhang, L. Rong, L. Wei, T. Gao and H. Bi (2026). Dual-configuration arabinogalactan-II synergizes with rhamnogalacturonan-I in Lycium barbarum pectin to construct an intestinal anti-inflammatory glycan scaffold. Carbohydr Polym. 381: 124914. https://doi.org/10.1016/j.carbpol.2026.124914

Li, J., Wang, T., Liu, F., Wang, J., Qiu, X. and Zhang, J. (2024a). Diagnostic test accuracy of cellular analysis of bronchoalveolar lavage fluid in distinguishing pulmonary infectious and non-infectious diseases in patients with pulmonary shadow. Front Med. 11:1–12. https://doi.org/10.3389/fmed.2024.1496088

Li, R., J. Li and X. Zhou (2024b). Lung microbiome: new insights into the pathogenesis of respiratory diseases. Signal Transduct Target Ther. 9: 19. https://doi.org/10.1038/s41392-023-01722-y

Liaqat, I., M.O. Omer, M.A. Rasheed and S. Raza (2024). Preparation, characterization and in vitro anticancer evaluation of albendazole-loaded zinc oxide nanoparticles. Pak Vet J. 44: 1343–1349. http://dx.doi.org/10.29261/pakvetj/2024.282

Liu, X and Z. Chen (2017). The pathophysiological role of mitochondrial oxidative stress in lung diseases. J Transl Med. 15: 207. https://doi.org/10.1186/s12967-017-1306-5

Mazumder, M.H.H and S. Hussain (2024). Air-pollution-mediated microbial dysbiosis in health and disease: Lung–gut axis and beyond. J Xenobiotics. 14: 1595–1612. https://doi.org/10.3390/jox14040086

Merchak, A and A. Gaultier (2020). Microbial metabolites and immune regulation: New targets for major depressive disorder. Brain Behav Immun Health. 9:100169. https://doi.org/10.1016/j.bbih.2020.100169

Moonwiriyakit, A., N. Pathomthongtaweechai and P.R. Steinhagen (2023). Tight junctions: From molecules to gastrointestinal diseases. Tissue Barriers 11: 114–146. https://doi.org/10.1080/21688370.2022.2077620

Mossman, B.T., M. Lippmann, T.W. Hesterberg, K.T. Kelsey, A. Barchowsky and J.C. Bonner (2011). Pulmonary endpoints (lung carcinomas and asbestosis) following inhalation exposure to asbestos. J Toxicol Environ Health. 14: 76–121. https://doi.org/10.1080/10937404.2011.556047

Mostafavi Abdolmaleky, H and J.R. Zhou (2024). Gut microbiota dysbiosis, oxidative stress, inflammation, and epigenetic alterations in metabolic diseases. Antioxidants 13:1–20. https://doi.org/10.3390/antiox13080985

Nadi, W.G., L.I. Ahmed, A.A.N. Awad and E.M. Taher (2015). Camara poisoning in cattle. Int J Vet Sci. 5: 231–233. https://doi.org/10.47278/journal.ijvs/2024.126

Neurath, M.F., D. Artis and C. Becker (2025). The intestinal barrier: A pivotal role in health, inflammation, and cancer. Lancet Gastroenterol Hepatol. 10: 573–592. http://dx.doi.org/10.1016/S2468-1253(24)00390-X

Otarov, Y., Z. Zharylkassyn, A. Shaibek, M. Mukasheva, Z. Sabirov, A. Alexeyev, A. Izdenov, C. Ismailov, M. Tilemissov, G. Dossybayeva, N. Zhaketayeva and U. Shaikhattarova (2025). Cytological analysis of upper respiratory tract epithelial cells in chrysotile asbestos factory workers. Life. 15: 1–10. https://doi.org/10.3390/life15030353

Pang, X., P. Huang, S. Huang and X. Liu (2025). The gut–lung axis: A new perspective on the impact of atmospheric particulate matter exposure on chronic obstructive pulmonary disease. Front Immunol. 16: 1–17. https://doi.org/10.3389/fimmu.2025.1657675

Portincasa, P., L. Bonfrate, M. Vacca, M. De Angelis, I. Farella, E. Lanza, M. Khalil, D.Q.H. Wang, M. Sperandio and A. Di Ciaula (2022). Gut microbiota and short chain fatty acids: Implications in glucose homeostasis. Int J Mol Sci. 23(3): 1-23. https://doi.org/10.3390/ijms23031105

Rumiyati, S., H. Kartikaningsih, D. Setijawati and H. Nursyam (2024). Qualitative analysis of *Caulerpa racemosa* chlorophyll extract in natural deep eutectic solvent (glucose-glycerol) using FTIR. Int J Agric Biosci. 13:295–300. https://doi.org/10.47278/journal.ijab/2024.121

Salonen, A., J. Nikkilä, J. Jalanka-Tuovinen, O. Immonen, M. Rajilić-Stojanović, R.A. Kekkonen, A. Palva and W.M. de Vos (2010). Comparative analysis of fecal DNA extraction methods. J Microbiol Methods. 81:127–134. https://doi.org/10.1016/j.mimet.2010.02.007

Shang, K., C. Ge, Y. Zhang, J. Xiao, S. Liu and Y. Jiang (2024). An evaluation of sex-specific pharmacokinetics and bioavailability of kokusaginine: an in vitro and in vivo investigation. Pharmaceuticals. 17(8): 1053-1071. https://doi.org/10.3390/ph17081053

Shukla, A., T.F. Barrett, K.I. Nakayama, K. Nakayama, B.T. Mossman and K.M. Lounsbury (2006). Transcriptional up-regulation of MMPs 12 and 13 by asbestos occurs via a PKCδ-dependent pathway in murine lung. FASEB J. 20:997–999. https://doi.org/10.1096/fj.05-4554fje

Smith, A.H and C.C. Wright (1996). Chrysotile asbestos is the main cause of pleural mesothelioma. Am. J. Ind. Med. 30:252–266. https://doi.org/10.1002/(SICI)1097-0274(199609)30:3<252

Strober, W and T. Watanabe (2011). NOD2, n intracellular innate immune sensor involved in host defense and Crohn ' s disease. Mucosal Immunol. 4(5): 484-495. https://doi.org/10.1038/mi.2011.29

Su, M., T. Tang, W. Tang, Y. Long, L. Wang and M. Liu (2023). Astragalus improves intestinal barrier function and immunity by acting on intestinal microbiota to treat T2DM: a research review. Front Immunol. 14: 1243834. https://doi.org/10.3389/fimmu.2023.1243834

Tulic, M.K., T. Piche and V. Verhasselt (2016). Lung-gut cross-talk: Evidence, mechanisms and implications. Clin Exp Allergy. 46:519–528. https://doi.org/10.1111/cea.12723

Ulluwishewa, D., R.C. Anderson, W.C. McNabb, P.J. Moughan, J.M. Wells and N.C. Roy (2011). Regulation of tight junction permeability by intestinal bacteria. J. Nutr. 141:769–776. https://doi.org/10.3945/jn.110.135657

Utembe, W. and Kamng'ona, A.W. (2024). Inhalation exposure to chemicals, microbiota dysbiosis and adverse effects. Sci Total Environ. 955:176938. https://doi.org/10.1016/j.scitotenv.2024.176938

Vemula, S., J. Mylaram, R. Yadala, G. Alla, A. Banothu and H.D. Veera (2024). Protective Effects of Naringenin on 5-Fluorouracil Induced Pulmonary Toxicity Via Modulation of NF-κB and Nrf2 Pathway. Pakistan Vet J. 44(1): 63-70. http://dx.doi.org/10.29261/pakvetj/2024.126

Wang, J., K. Li, D. Hao, X. Li, Y. Zhu, H. Yu and H. Chen (2024a). Pulmonary fibrosis: pathogenesis and therapeutic strategies. Med Comm. 5(10):1–27. https://doi.org/10.1002/mco2.744

Wang, J., J. Luo, D. Rotili, A. Mai, C. Steegborn, S. Xu and Z. G. Jin (2024b). SIRT6 Protects Against Lipopolysaccharide-Induced Inflammation in Human Pulmonary Lung Microvascular Endothelial Cells. Inflammation. 47(1): 323–332. https://doi.org/10.1007/s10753-023-01911-5

Wang, Y., P. Wang, S. Yuan, X. Du, R. Yan, X. Wang, Y. Hu, S. Pu, Y. Shen, Y. Fang and X. Zhou (2025). Reversal of BCAA-driven inflammatory senescence by traditional herbal oil prevents atopic dermatitis relapse. Phytomedicine. 148: 157425. https://doi.org/10.1016/j.phymed.2025.157425

Xu, Y., R. Xie, Y. Weng, Y. Fang, S. Tao, H. Zhang, H. Chen, A. Han, Q. Jiang and W. Liang (2025). Role and mechanism of gut microbiota-host interactions in Crohn's disease. Int J Colorectal Dis. 40:130. https://doi.org/10.1007/s00384-025-04917-7

Xu J., J. Sui, Y. Luo, Q. Zhao, W. Bi, H. Duan, Y. Fu, Q. Yang, J. Sun, F. Dai, X. Gu, Y. Wu and W. Qu (2025). The protective and therapeutic effects of herbal medicines on hepatic disorders in animals. Pak Vet J. 45(4): 1491-1502. http://dx.doi.org/10.29261/pakvetj/2025.324

Yan, Q., S. Jia, D. Li and J. Yang (2023). The role and mechanism of action of microbiota-derived short-chain fatty acids in neutrophils. Biomed. Pharmacother. 169:115821. https://doi.org/10.1016/j.biopha.2023.115821

Moldoveanu, B., P. Otmishi, P. Jani, J. Walker, X. Sarmiento, J. Guardiola, M. Saad and J. Yu (2009). Inflammatory mechanisms in the lung. J Inflamm Res. 2:1-11. https://doi.org/10.2147/jir.S4385

Zandwijk, N. van, Frank, A.L., Reid, G., Røe, O.D. and Amos, C.I. (2024). Asbestos-related lung cancer: An underappreciated oncological issue. Lung Cancer. 194: 107861. https://doi.org/10.1016/j.lungcan.2024.107861

Zhan, K., X. Gong, Y. Chen, M. Jiang, T. Yang and G. Zhao (2019). Short-chain fatty acids regulate immune responses via G protein-coupled receptor 41 in Bovine Rumen Epithelial Cells. Front Immunol. 10:1–11. https://doi.org/10.3389/fimmu.2019.02042

Zmora, N., M. Levy, M. Pevsner-Fishcer and E. Elinav (2017). Inflammasomes and intestinal inflammation. Mucosal Immunol. 10:865–883. doi: 10.1038/mi.2017.19